Research Article

The Journal of Comparative Neurology
Research in Systems Neuroscience
DOI 10.1002/cne.23041

Title: Efferent Projections of C3 Adrenergic Neurons in the Rat Central Nervous System

Authors: Charles P. Sevigny[1], Jaspreet Bassi[1], David A. Williams[1], Colin R. Anderson[2], Walter G. Thomas[3], Andrew M. Allen[1,4]

[1]Department of Physiology, The University of Melbourne, Melbourne, Victoria, Australia

[2]Department of Anatomy and Cell Biology, The University of Melbourne, Melbourne, Victoria, Australia

[3]School of Biomedical Sciences, The University of Queensland, Queensland, Australia

[4]Florey Neurosciences Institutes, The University of Melbourne, Melbourne, Victoria, Australia,

Running Head: Efferent Projections of C3 Neurons in the Rat

Associate Editor: Paul E. Sawchenko

Key Words: autonomic regulation, lentivirus, sympathetic preganglionic neurons, phenylethanolamine N-methyltransferase, catecholamines

Corresponding Author: A. Prof. Andrew M. Allen, Department of Physiology, The University of Melbourne, Victoria 3010, Australia. Telephone: +61 3 8344 5838; Facsimile: +61 3 8344 5818; email: a.allen@unimelb.edu.au

This work was supported by funding from the Australian Research Council (DP1094301) and the Australian National Health and Medical Research Council (#566536). C.P.S. is the recipient of a NHMRC Dora Lush Postgraduate Scholarship.

Received: Aug 09, 2011; Revised: Dec 19, 2011; Accepted: Jan 07, 2012

Abstract

C3 neurons constitute one of three known adrenergic nuclei in the rat central nervous system (CNS). While the adrenergic C1 cell group has been extensively characterized both physiologically and anatomically, the C3 nucleus has remained relatively obscure. This study employed a lentiviral tracing technique which expresses green fluorescent protein behind a promoter selective to noradrenergic and adrenergic neurons. Microinjection of this virus into the C3 nucleus enabled the selective tracing of C3 efferents throughout the rat CNS, thus revealing the anatomical framework of C3 projections. C3 terminal fields were observed in over forty different CNS nuclei, spanning all levels of the spinal cord, as well as various medullary, mesencephalic, hypothalamic, thalamic, and telencephalic nuclei. The highest densities of C3 axon varicosities were observed in Lamina X and the intermediolateral cell column of the thoracic spinal cord, as well as the dorsomedial medulla (both commissural and medial nuclei of the solitary tract, area postrema, and the dorsal motor nucleus of the vagus), ventrolateral periaqueductal gray, dorsal parabrachial nucleus, periventricular and rhomboid nuclei of the thalamus, and paraventricular and periventricular nuclei of the hypothalamus. In addition, moderate and sparse projections were observed in many catecholaminergic and serotonergic nuclei, as well as the area anterior and ventral to the third ventricle, Lamina X of the cervical, lumbar and sacral spinal cord, and various hypothalamic and telencephalic nuclei. The anatomical map of C3 projections detailed in this survey hopes to lay the first steps towards developing a functional framework for this nucleus.

Introduction

C3 neurons of the rostral dorsomedial medulla constitute one of three known adrenergic nuclei in the rat central nervous system (CNS), characterized by their expression of all the catecholamine-synthesizing enzymes, including tyrosine hydroxylase (TH), dopamine-β-hydroxylase, and phenylethanolamine N-methyltransferase (PNMT). While their counterparts, the C1 neurons, have been widely studied due to their role in regulating sympathetic vasomotor activity (Card et al., 2006; Guyenet, 2006; Reis et al., 1989; Stornetta, 2009), the C3 cell group, which constitutes approximately 15% of all adrenergic neurons in the rat CNS (Minson et al., 1990), has yet to be investigated in detail.

The C3 nucleus is a medullary midline structure in the medial longitudinal fasciculus which spans from the ventral surface of the fourth ventricle to the dorsal tip of raphe obscurus, and rostro-caudally between the caudal tip of the dorsal paragigantocellular nucleus and the rostral extent of the hypoglossal nucleus. These cells were first characterized as adrenergic (Hokfelt et al., 1973) and have since been shown to express the vesicular glutamate transporter 2 (VGluT2), suggesting they are glutamatergic (Stornetta et al., 2002). Subpopulations of C3 neurons co-express neuropeptide Y mRNA (Stornetta et al., 1999), glucocorticoid receptor immunoreactivity (Sawchenko and Bohn, 1989), and cocaine and amphetamine related transcript (CART) immunoreactivity (Wittmann et al., 2004). Various retrograde tracing studies have identified that subsets of C3 neurons project to the thoracic spinal cord (Minson et al., 1990), paraventricular nucleus of the thalamus (PVT; Otake and Ruggiero, 1995; Phillipson and Bohn, 1994), paraventricular, supraoptic, and tuberomamillary nuclei of the hypothalamus (Cunningham et al., 1990; Ericson et al., 1989), dorsal raphe nucleus (Peyron et al., 1996), periaqueductal gray (PAG; Herbert and Saper, 1992), ventral tegmental area (Mejias-Aponte et al., 2009), and locus coeruleus (Pieribone et al., 1988). Physiologically, C3 neurons increase expression of the immediate early gene Fos during depressor responses elicited by sodium nitroprusside (Murphy et al., 1994), but not during hemorrhage (Dun et al., 1993). This collection of studies implicates the C3 cell group as an autonomic integration center, but stops short of providing a comprehensive overview of the anatomical distribution of C3 processes.

The purpose of the current study is to map C3 efferents throughout the rat central nervous system by microinjecting a lentivirus designed to induce expression of green fluorescent protein (GFP)

selectively in cells of a noradrenergic or adrenergic phenotype. This anatomical survey reveals C3 efferents extending to a multitude of nuclei beyond those previously identified, and provides a detailed anatomical framework to further our understanding of this cell group's role within the central nervous system.

Materials and Methods

Lentivirus Preparation

Lentivirus expressing GFP under the control of a multimeric *Phox2* binding site promoter (LV.PRSx8.EGFP; Hwang *et al*., 2001), was prepared using methods previously described (Coleman et al., 2003; Sevigny et al., 2008; Teschemacher et al., 2005).

Animals

All *in vivo* experiments were conducted in accordance with the Australian National Health and Medical Research Council 'Code of Practice for the Care and Use of Animals for Scientific Purposes' and were approved by the University of Melbourne Animal Experimentation Ethics and Biosafety Committee. Seven male Sprague Dawley rats (300-400g) were used for this study. Animals were obtained from the University of Melbourne Biological Resources Facility, and housed with a 12-h light : dark cycle at a constant temperature (22 ± 1°C) with *ad libitum* access to standard rat chow and water.

Microinjection of Lentivirus into the C3 Region

Rats were injected with a non-steroidal, anti-inflammatory agent (meloxicam, 1 mg/kg, s.c.; Metacam, Boehringer Ingelheim, NSW, Australia) prior to lentiviral injection protocol. For all surgical protocols (including transcardial perfusions), animals were first lightly anesthetized by inhalation of isofluorane (Rhodia Australia Pty, Notting Hill, Vic., Australia) prior to intramuscular injection of a mixture of ketamine (60 mg/kg; Lyppard, Dingley, Vic., Australia) and medetomidine (250 mg/kg, ; Pfizer Animal Health, West Ryde, NSW, Australia). After a deep plane of anesthesia was evidenced by loss of pedal withdrawal and corneal reflexes, animals were placed in a stereotaxic frame with the skull angled downwards 40°. An incision was made along the midline and muscles separated to expose the atlanto-occipital membrane. A small portion of the occipital bone (1-2mm) was removed by trepination, and the atlanto-occipital membrane opened to expose calamus scriptorius, which was used as a reference point for stereotaxic coordinates. Lentiviral solution was injected from a glass micropipette (20–50

μm tip diameter) using a picospritzer (World Precision Instruments, Sarasota, FL, USA), and volume of injectate was determined by measuring the movement of the fluid meniscus with a monocular microscope containing an eyepiece graticule. A series of injections (100nl per injection, viral titre $0.75x10^{10}$viral particles/ml) were made along the midline at the following coordinates: -0.8 and -1.4mm DV each at 1.6, 1.9, 2.2, 2.4, and 2.6mm rostral to calamus scriptorius. The incision was then sutured, and animals revived via an intramuscular injection of atipamazole (1 mg/kg; Pfizer Animal Health, West Ryde, NSW, Australia). 4 of 7 injected animals were allowed to recover for 3 weeks in their home cages. However, subsequent histology revealed this recovery time was not adequate for the desired expression and transport of GFP. The next 3 animals were allowed to recover for 5 weeks in their home cages, which provided adequate expression of GFP in the sacral spinal cord (the greatest distance from the injection site). After the specified time, animals were anesthetized as described earlier, and killed by transcardial perfusion with 50ml of 0.9% saline followed by 500ml of 4% formaldehyde in 0.1 M phosphate buffer. Brains and spinal cords were removed and postfixed with 4% formaldehyde in 0.1 M phosphate buffer for 1 day in preparation for histological protocols.

Histology

Postfixed tissue was transferred to a 30% sucrose solution for 1 day prior to sectioning. Brains were bisected along the coronal plane 8mm from the caudal end of the brain matrix (approximately 1mm rostral to the cerebellar peduncle). Spinal cords were blocked transversely into sections containing 3-4 spinal segments. All tissue was snap frozen in isopentane on dry ice before being sectioned on a cryostat either coronally (brain) or horizontally (spinal cord) at a thickness of 40μm. Horizontal segments of spinal cord were sectioned at a slight oblique angle (3-7°) to ensure visualization of multiple structures within a single section. All tissue was stored free-floating in cryoprotectant (30% sucrose, 30% ethylene glycol, 1% polyvinyl-pyrrolidone in 50mM phosphate buffer, pH 7.2) at -20°C until subsequent immunohistochemical procedures.

Immunohistochemistry and Nissl Stains

Nissl stains were performed on coronal brain sections sampled every 240µm using thionin solution to identify landmarks for mapping purposes (detailed below). Immunohistochemistry methods followed those detailed by Llewellyn-Smith et al., (2003). Briefly, coronal sections of brain were sampled every 240µm, and horizontal sections of spinal cord every 160µm. Sections were rinsed in tris-buffered saline with 0.05% merthiolate, pH 7.4 (TBS), then transferred to blocking solution (10% normal horse serum, 0.3% Triton in TBS) for 30 minutes at room temperature (T°). Sections were then incubated in a primary antibody cocktail (containing multiple antibodies where appropriate) diluted in blocking solution for 72 hours at T°, after which they were rinsed in TBS. Sections were then incubated for 24 hours at T° in a secondary antibody cocktail (containing multiple antibodies where appropriate) diluted in a modified blocking solution (1% normal horse serum, 0.3% Triton in TBS). Where appropriate, tissue incubated with biotinylated secondary antibodies were subsequently rinsed and incubated for two hours at T° in a fluorophore conjugated streptavidin. All primary and secondary antibodies used, along with concentrations, sources, and catalog numbers are listed in Table 1. Note that for double-labeling with GFP and choline acetyltransferase (ChAT), secondary antibodies were applied sequentially (donkey anti-goat Cy5, followed by goat anti-chicken Alexa 488) to avoid possible cross-binding between the secondary antibodies. Using this sequential application of antibodies did not result in any colocalization between GFP-ir and ChAT-ir elements. Sections were finally rinsed in TBS, transferred to 0.1M phosphate buffer, and mounted onto gelatin coated slides. Slides were coverslipped using Cytoseal (JMS-Cole Parmer, Balwyn, VIC, Australia) to preserve fluorescence.

Antibody Characterisation

Table 1 provides a list and relevant details of all antibodies used in immunohistochemistry protocols. The GFP antibody was tested by the manufacturer by Western blot analysis and immunoprecipitation of transgenic mouse spinal cords. It recognizes a single 27kDa band and application of this antibody to tissue from wild-type animals yielded no labeling (Enjin et al., 2010). The TH antibody recognizes a single 60kDa band during Western blot analysis on PC12 lysates as detailed by the manufacturer. Labelling observed using this antibody in the current study yielded the same patterns as previous reports (Stornetta et al., 2002). The tryptophan hydroxylase (TrOH) antibody yielded a single band at 55kDa during Western blot analysis of

rabbit pineal gland extract (manufacturer), and yielded labeling which corresponded to known distributions of serotonergic neurons (Liu and Wong-Riley, 2010).The ChAT antibody detects a single 70kDa product in Western blot analysis of rat brain extract (manufacturer), and yielded labeling which corresponds to patterns observed in previous reports (Gaillard et al., 2008). The specificity of the vesicular monamine transporter 2 (VMAT2) antibody was determined through selective transfection of monkey kidney fibroblasts (CV-1 cells) with either rat VMAT1 or rat VMAT2 clones. Transfection and functionality of the VMATs were determined via tritiated serotonin uptake, and immunolabeling for VMAT2 was restricted to the VMAT2 transfected CV-1 cells, and absent in the control and VMAT1 transfected lines (Weihe et al., 1994). Labeling was abolished in sections reacted with primary antibody preabsorbed with excess VMAT2 antigen compared with labeled sections reacted with untreated primary antibody (Weihe et al., 2005). Immunolabeling with the VMAT2 antibody in the rat CNS as reported by Weihe et al. (1994) coincided with previous reports of VMAT2 distribution by *in situ* hybridization histochemistry and northern blot analysis (Erickson et al., 1992; Liu et al., 1992). The VGluT2 antibody labels a single 62kDa band in Western blot analysis of astrocytes from rat visual cortex (Montana et al., 2004), and preadsorbtion with the immunogen peptide abolishes labeling in nerve terminals (Masterson et al., 2009).

Bright Field and Fluorescent Microscopy

Bright field (Nissl stained sections) and fluorescent (injection sites) microscopy was performed using an Axio Imager D.1 microscope connected to an AxioCam MRc5 digital camera (Zeiss Microimaging, Germany). Viral injection sites were confirmed using immunofluorescence for GFP immunoreactivity (GFP-ir) and TH-ir to confirm location and specificity of expression in catecholaminergic neurons.

Confocal Microscopy

Sections were viewed with a Zeiss LSM 510 META confocal microscope. Images were acquired with either a 40x IR-Achroplan (NA 0.80) water immersion objective or a 100x IR-Achroplan (NA 1.25) oil immersion objective. All sections labeled with multiple fluorescent probes were

scanned using settings adjusted to eliminate emission crosstalk between channels. Alexa 488-conjugated fluorescent probes, Cy3-conjugated probes, and Cy5-conjugated probes were excited at 488 nm (100 mW argon ion laser), 543 nm (10 mW green helium neon laser) and 633 nm (10 mW red helium neon laser), respectively.

Image Post-Processing

Low magnification Nissl stained images were adjusted for brightness where appropriate using Adobe Photoshop. Where appropriate, confocal microscopy images were adjusted only for contrast using LSM Image Browser version 4.0.0.241 (Zeiss Microimaging, Germany).

Mapping of C3 Processes

For mapping purposes, Nissl stained sections of brain were sampled from a series immediately adjacent to those labeled for GFP-ir, enabling structural identification of regions observed to contain GFP-ir processes. Fluorescently labeled sections were systematically surveyed for GFP-ir processes using the confocal microscope. Any region containing GFP-ir processes was imaged, and the imaged region annotated on the corresponding adjacent Nissl stained image. The tissue was then surveyed again using the fluorescent microscope to ensure all GFP-ir processes had been accounted for. Spinal cord tissue was surveyed using bright field microscopy for structural identification and fluorescent microscopy to identify regions containing GFP-ir processes. After mapping these sections, GFP-ir processes were imaged using confocal microscopy.

For summary purposes, semi-quantitative analysis was performed based on comparative observations between projection sites, as listed in Table 2. Regions containing C3 varicosities were ranked +, + +, + + +, or + + + + based on relative observed densities of varicose fields, where "+" indicates a field containing sparse yet consistent varicosities, and "+ + + +" represents the densest observed fields. Some specific examples of each ranking can be observed in the confocal micrographs within the figures: +: Figure 6D (lateral hypothalamus), + +: Figure 3C

(rostral ventrolateral medulla), + + +: Figure 3H (dorsal motor nucleus of the vagus), and + + + +: Figure 3G (area postrema).

Results

Injection Sites

The lentiviral injection protocol outlined in this study resulted in GFP-ir expression in 79 ± 3% of TH-ir neurons within the C3 region (Figure 1). GFP-ir C3 neurons were observed across the full rostral-caudal extent of the region for all injections, with little variability in labeling percentage as described above. We did not observe GFP-immunoreactivity in neurons that were not TH-ir. As the C3 nucleus does not overlap with any other catecholaminergic or *Phox2* expressing cell group, viral expression was deemed to be selective to C3 neurons; GFP labeling was not observed in the nearby adrenergic C2 nucleus, or the noradrenergic A2 nucleus. Infected neurons were generally multipolar and ellipsoidal or triangular in shape, with nearby GFP-ir processes possibly extending to the surface of the fourth ventricle (Figure 3B).

General Observations

GFP-ir processes were found in many locations throughout the central nervous system as detailed below. Reported regions were those containing GFP-ir terminal-like axon varicosities (distinct bulges along or at the ends of axons), whereas regions containing no GFP immunoreactivity, or those containing only axons of passage (displaying no varicosities) were generally not reported.

GFP-ir varicose C3 processes were observed in more than 40 different regions of the CNS. Across these regions, the density of processes varied from only one or two branching collaterals to dense, elaborate arborisations overlapping with the majority of the targeted area. The following section will begin by describing the regions receiving the densest projections, followed by moderately innervated regions, sparsely innervated regions, and finally regions known to contain PNMT-ir processes which appear not to originate from C3 neurons.

Densely Innervated Regions

The most dense innervation is observed throughout the intermediolateral cell column (IML; Lamina IX) of the spinal cord, reaching its highest density in the mid-thoracic segments (Figure 2E-K). Co-labeling for ChAT-ir revealed that this bundle of axons provides dense collaterals and varicosities in the region of ChAT-ir sympathetic preganglionic neuronal clusters (SPGNs;

Figure 2F). Within these clusters, GFP-ir varicosities are also immunoreactive for VMAT2, and VGluT2 (Figure 2G-K), implicating them in the release of both catecholamines and glutamate. An additional column of spinal processes were observed throughout Lamina X, clustered around the central canal from upper cervical, through to sacral levels of the spinal cord, reaching a peak density at the mid-thoracic segments (Figure 2A-D). These processes formed densely interwoven networks displaying numerous axon varicosities which invariably overlapped with ChAT-ir neurons or processes. Interestingly, the processes within Lamina X appeared to be of a smaller axon diameter than those which innervate the IML, implying a potential variability in conduction velocity between these two branches of collaterals.

Within the brain, high densities of C3 processes were observed in several regions within the medulla oblongata, mesencephalon, and diencephalon. In the dorsal medulla, the most dense fields of C3 processes were contained in the commissural and medial portions of the nucleus of the solitary tract (NTS), area postrema (AP), and the dorsal motor nucleus of the vagus (DMX; Figure 3). Co-labeling of these regions with markers for TH and ChAT, revealed that the processes in the NTS at least partially overlap with TH-ir C2 adrenergic neurons and their processes (Figure 3A), as well as the ChAT-ir parasympathetic preganglionic neurons in DMX (Figure 3H).

Within the midbrain, C3 processes densely innervate the entire ventrolateral periaqueductal gray (vlPAG), with elaborately branching collaterals (Figure 4A). The nearby lateral and medial parabrachial nuclei also contained a high density of C3 terminal branches with the appearance of more varicosities amongst that process in the lateral division. In the lateral division GFP-ir axons contribute to densely clustered TH-ir fibers forming fine “baskets” outlining somata (Figure 4F-G).

One of the densest fields of C3 collaterals occurred within the thalamus. Here, GFP-ir processes innervate a rostral-caudal expanse of over 3mm from Bregma -0.8mm to -4.0mm, encompassing the full extent of the mediodorsal and paraventricular nuclei (Figures 5A-B and 6C), as well as the rhomboid nucleus (data not shown). Also within the diencephalon, C3 processes were observed throughout many hypothalamic regions, with the highest density of varicosities confined to the paraventricular and periventricular hypothalamic nuclei (Figure 6A, F, and H).

Moderately Innervated Regions

The largest classification of observed regions is those receiving what were deemed to have moderate innervation. Within the medulla, these regions include the rostral ventrolateral medulla (RVLM), and the caudal ventrolateral medulla (CVLM). Sections co-labeled for TH-ir reveal that C3 processes appear in close proximity to C1 adrenergic neurons in the RVLM (Figure 3C), as well as the noradrenergic A1 neurons of the CVLM (Figure 3I).

Several mesencephalic nuclei also received moderate projections from C3 neurons. When this tissue was co-labeled with markers for TH-ir and TrOH-ir, GFP-ir processes appeared to be specifically projecting to the region of serotonergic B6/B7 neurons of the dorsal raphe nucleus, as well as the noradrenergic A7, A6, and A10 neurons of the Kölliker Fuse nucleus (Figure 4E), locus coeruleus (Figure 4H), and the ventral tegmental area (Figure 4D), respectively. Moderate innervation was also observed in the lateral (data not shown) and superoculomotor (Figure 4C) subdivisions of the PAG.

Moderate innervations of the diencephalon were mainly restricted to the hypothalamus and AV3V (the region anterior and ventral to the third ventricle). A moderately dense projection was also observed in the suprachiasmatic (data not shown), supraoptic (Figure 6E), retrochiasmatic (Figure 6B), dorsomedial (Figure 5D), arcuate (Figure 3I) and terete (Figure 5G) nuclei. Within AV3V, moderate numbers of processes were observed within the median and medial preoptic nuclei (Figure 7B-C), and the organum vasculosum of lamina terminalis (OVLT; Figure 7D).

Within other regions of the telencephalon a moderate density of GFP-ir processes is observed in the medial amygdala (Figure 5H), and globus pallidus (data not shown). When combined with TH-ir, GFP-ir fibers within globus pallidus appear to contribute to TH-ir “fiber baskets” surrounding neuronal somata, as also observed in the medial parabrachial nucleus. These fibers display very few apparent varicosities, but nevertheless appear to form intimate relationships with cell bodies in the region.

Sparsely Innervated Regions

An assortment of additional regions receives sparse projections from C3 neurons. While these regions generally contain only one or two branching varicose axons, similar projections were

observed across all animals in the study. How much influence such modest innervations provide is a point for the discussion, but the consistency across animals makes the observation worth reporting.

Within the raphe pallidus C3 processes appear to target the serotonergic B1 neurons in sections co-labeled with TrOH-ir (Figure 3F), as well as the B2 neurons of raphe obscurus (Figure 3E), and B3 neurons within raphe magnus (Figure 4I). In the diencephalon, GFP-ir varicose axons are observed in the lateral hypothalamus (Figure 6D), arcuate nucleus (Figure 6I), median eminence (Figure 6G), medial tuberal nucleus (Figure 5F), and the bed nucleus of stria terminalis (Figure 7A). The most rostral projections of C3 neurons were found in the olfactory tubercule, with isolated axon varicosities appearing in the islands of Calleja, along the ventromedial surface between bregma 2.52 and 1.68 (data not shown). Projections were also seen in the lateral septal nucleus at bregma 0.96, and the horizontal diagonal band (bregma 0.96-0.72, data not shown).

Non-Innervated Regions

When compared to overall distribution of PNMT in the rat brain as described by Björklund and Hökfelt (1984), there are several regions which contain PNMT-ir varicosities that can be said *not* to originate from C3 neurons. While many of these regions are reported to contain only sparse fibers, those which contain a moderate or high density of PNMT-ir fibers which do not originate from C3 neurons include the supramamillary region of the diencephalon, the mesencephalic central superior nucleus, superior olive, corpus trapezoideum, and A5 nuclei, the Purkinje cell layer of the cerebellum, and the pyramidal tract and intercalated nucleus within the medulla. Notably, Card et al. (2006) did not report these regions among those receiving projections from C1 neurons either.

Table 2 provides a semi-quantitative overview of regions observed to contain C3 varicose processes based on relative observations. The table compares these contributions with the framework for overall PNMT distribution throughout the CNS as detailed by Björklund and Hökfelt (1984), and contributions of C1 adrenergic neurons, as described by Card et al. (2006). It should be noted that these comparisons were made after data analysis for C3 projections had been completed, and all regions containing C3 processes fit into the overall PNMT framework.

Confirmation of Axon Varicosities as Release Sites

Several key regions were co-labeled with markers of the presynaptic vesicular transporters VMAT2 and VGluT2 as confirmation of vesicular release of catecholamines or glutamate, respectively. Many GFP-ir axon varicosities in the thoracic IML were also immunoreactive for both VMAT2 and VGluT2 (Figure 2G-K). In addition, double-labeling experiments revealed co-localization of GFP-ir and VGluT2 ir in varicosities within all regions examined, including DMX (Figure 8A-C), PVT (Figure 8D-F), PVN (Figure 8G-I), and AP (Figure 8J-L).

Discussion

This anatomical survey reveals a variety of nuclei targeted by C3 projections, which carry a range of functional implications for these neurons. C3 neurons project to regions known to regulate both the sympathetic and parasympathetic branches of the autonomic nervous system, nociception and analgesia, fluid and metabolic homeostasis, as well as stress and defense responses. While all of these systems are woven together by established pathways and regulatory effects, it appears that C3 neurons have a broad influence over all these systems via direct projections to key regions such as AV3V, hypothalamus, thalamus, and both medullary and spinal regions regulating sympathetic and parasympathetic motor outflow. While existing literature tells us little of their physiology, this study which details their CNS circuitry may reveal potential functional roles for C3 neurons.

The lentiviral tracing technique employed in this study offers several distinct advantages over traditional anterograde tracing methods. Primarily, the phenotype specific promoter within the viral plasmid limits GFP expression to neurons expressing *Phox2*, a transcription factor essential to the development of noradrenergic and adrenergic neurons. While *Phox2* is not limited to (nor)adrenergic neurons, within the C3 region all *Phox2* expressing neurons have been shown to be catecholaminergic (Card et al., 2010), meaning labeled terminals can be associated specifically with C3 neurons, as opposed to all neurons within the region. The cells may be distinguished by targeted injections and confirmed with post hoc immunohistochemical analysis. We were able to confirm this specificity by observing GFP-ir exclusively in TH-ir neurons. Secondly, GFP was expressed in approximately 70-80% of the targeted neurons, which is a vast improvement over labeling rates of most anterograde tracers. This enables a more robust and thorough exploration of the processes originating from these neurons and increases confidence that regions not containing GFP labeled processes aren't simply a result of insufficient labeling of the original population. Lastly, once neurons of the correct phenotype have been infected with the virus, they continue to produce GFP, which is transported throughout the neuron. This provides a more abundant label for immunohistochemistry as opposed to a chemical tracer which is limited in quantity by the original injection and uptake. These factors have enabled this survey to identify GFP-ir processes throughout the CNS which have originated specifically from a majority of C3 neurons.

Due to their dense innervation of SPGNs within the IML, C3 neurons are likely to function as sympathetic pre-motor neurons, potentially influencing a variety of general visceral efferents. While this study did not investigate which functional subtypes of SPGNs were innervated, transneuronal labeling studies have shown a polysynaptic pathway leading from C3 neurons to the stellate ganglion (Jansen et al., 1995), testes (James et al., 2008), and spleen (Cano et al., 2001), with no labeling of C3 neurons reported following pseudorabies virus infection of renal postganglionic neurons (Schramm et al., 1993). Fields of C3 axon varicosities were also found in several medullary autonomic regions including the RVLM, CVLM, raphe pallidus, and raphe obscurus, with the densest fields in the medulla observed within AP, DMX, and both medial and commissural parts of the NTS. Within RVLM and CVLM, C3 processes were observed forming apparent close appositions with adrenergic C1 neurons and noradrenergic A1 neurons. The RVLM, CLVM, and NTS have been extensively characterized as regions responsible for sympathetic vasomotor outflow (Guyenet, 2006), neuroendocrine regulation (Blessing and Willoughby, 1985; Pilowsky et al., 1987), and viscerosensory processing, respectively (Boscan et al., 2002), as well as their role in baroreflex circuitry (Chan and Sawchenko, 1998). In conjunction with the projections to the IML, these observations suggest that C3 neurons could play a pivotal, unexplored role in regulation of sympathetic outflow.

C3 neurons are also labeled following transynaptic tracing of the parasympathetic innervation of the pancreas (Loewy et al., 1994). Our data indicate this to be a direct pathway based on an overlap of densely clustered C3 varicosities with ChAT-ir motor neurons within DMX, suggesting a functional role in parasympathetic modulation in addition to the sympathetic targets described above. Whilst PNMT-ir fibers have been shown to form (presumably inhibitory) symmetric synapses with parasympathetic preganglionic neurons in DMX (Pickel et al., 1986), this study indicates that GFP-ir varicosities within DMX are glutamatergic. Within the hypothalamus and lamina terminalis, C3 varicosities were observed within nuclei known to project (often reciprocally) to the medullary autonomic regions outlined above. These varicosities were within the parvicellular part of the paraventricular nucleus of the hypothalamus (PVN), the medial preoptic nucleus, and OVLT. Together these observations indicate a strong association of C3 neurons with regulation of cardiovascular and homeostatic facets of autonomic function.

C3 neurons are known to contribute to regulation of the hypothalamic-pituitary-thyroid axis metabolic regulatory pathway. Studies have shown that a subset of C3 terminals within the PVN contain CART-ir, and closely oppose thyroidotropin releasing hormone immunoreactive neurons (Wittmann et al., 2004). This pathway is believed to be responsible for feeding responses and energy homeostasis. These PNMT-ir terminals have also been shown to form asymmetric synapses with parvicellular PVN neurons and to contain NPY (Alonso, 1993; Wittmann et al., 2002), which is known to inhibit indirectly the hypothalamic-pituitary-thyroid axis (Fekete et al., 2001). Thus, a subset of the C3 varicosities we observed within the PVN could have a regulatory role in metabolic homeostasis.

The PVT encompasses one of the densest clusters of C3 axon varicosities in the brain. Indeed this region has been previously reported as not only containing PNMT-ir processes (Hokfelt et al., 1973), but also receiving monosynaptic inputs from C1-3 neurons (Otake and Ruggiero, 1995; Phillipson and Bohn, 1994). In addition, many regions which project to the PVT also contain PNMT-ir varicosities, forming several disynaptic pathways between medullary adrenergic cell groups and the PVT (Otake et al., 1995). These regions include many which contain varicose projections from C3 neurons, such as the medial amygdala, bed nucleus of stria terminalis, PVN, suprachiasmatic nucleus, paraventricular nucleus of the hypothalamus, dorsomedial hypothalamus, lateral hypothalamus, medial preoptic nucleus and median preoptic nucleus. This outlines a set of convergent projections from C3 to PVT composed of disynaptic and monosynaptic pathways. Given that stimulation of the PVT can induce defense responses (Hilton and Redfern, 1986), its responsiveness to a variety of stressors (Chastrette et al., 1991; Imaki et al., 1993; Sharp et al., 1991), and its intimate relationship with the hypothalamic-pituitary-adrenal axis via the monosynaptic pathway from PVN, ascending C3 collaterals could be relaying visceral information to this region which in turn contributes to defensive responses to stressful stimuli.

The hypothalamic-pituitary-adrenal (HPA) axis could also receive direct input from C3 neurons. Given the interaction between medullary PNMT-ir fibers and corticotropin-releasing hormone immunoreactive parvicellular neurons within the PVN described by Wittmann et al. (2004), it is likely that the C3 varicosities observed in the current study are influencing this key component of the stress pathway. In addition to direct interaction within the PVN, C3 varicosities were also

observed in brain regions known to project to the PVN component of the HPA axis, namely, the NTS, locus coeruleus, and the bed nucleus of stria terminalis. Much like the thalamic convergence mentioned earlier, these multidimensional inputs into the HPA axis suggest a potential modulating role for C3 neurons within the stress response.

While existing literature helps to develop functional possibilities for some of the observed C3 projections, many remain unresolved. For example, the dense projections which innervate Lamina X throughout all levels of the spinal cord and the robust innervations of the vlPAG could either suggest a role in nociception and analgesia (Cavun et al., 2004; Dean, 2005; Nahin et al., 1983; Palazzo et al., 2010; Tjen et al., 2006), or autonomic regulation (Llewellyn-Smith, 2009; Pelosi et al., 2008). In addition to the regions containing a high density of C3 projections, the many nuclei which contain only one or two varicose axons remain a functional mystery. Given that these projections were observed consistently across all animals, they may carry some functional relevance, despite their limited anatomical presence. Perhaps delivering a signal to a limited number of cells in these regions allows C3 neurons to modulate certain nuclei subtly while simultaneously activating other, more densely innervated regions with robust excitatory drive. While this survey can only offer functional speculation, the high number of regions receiving projections from C3 neurons, coupled with the density of these projections in key autonomic centers, suggests that this underexplored cluster of adrenergic neurons plays a larger role in autonomic regulation than previously considered.

Other Acknowledgements:

The authors thank Mr. D.A. Carter for technical assistance.

Literature Cited:

Alonso G. 1993. Differential organization of synapses immunoreactive to phenylethanolamine-N-methyltransferase or neuropeptide Y in the parvicellular compartments of the hypothalamic paraventricular nucleus of the rat. J Chem Neuroanat 6(2):55-67.

Björklund A, Hökfelt T. 1984. Handbook of chemical neuroanatomy. Amsterdam ; New York: Elsevier. 157-276 p.

Blessing WW, Willoughby JO. 1985. Inhibiting the rabbit caudal ventrolateral medulla prevents baroreceptor-initiated secretion of vasopressin. J Physiol 367:253-265.

Boscan P, Pickering AE, Paton JF. 2002. The nucleus of the solitary tract: an integrating station for nociceptive and cardiorespiratory afferents. Exp Physiol 87(2):259-266.

Cano G, Sved AF, Rinaman L, Rabin BS, Card JP. 2001. Characterization of the central nervous system innervation of the rat spleen using viral transneuronal tracing. J Comp Neurol 439(1):1-18.

Card JP, Sved JC, Craig B, Raizada M, Vazquez J, Sved AF. 2006. Efferent projections of rat rostroventrolateral medulla C1 catecholamine neurons: Implications for the central control of cardiovascular regulation. J Comp Neurol 499(5):840-859.

Card JP, Lois J, Sved AF. 2010. Distribution and phenotype of Phox2a-containing neurons in the adult sprague-dawley rat. J Comp Neurol 518(12):2202-2220.

Cavun S, Goktalay G, Millington WR. 2004. The hypotension evoked by visceral nociception is mediated by delta opioid receptors in the periaqueductal gray. Brain Res 1019(1-2):237-245.

Chan RK, Sawchenko PE. 1998. Organization and transmitter specificity of medullary neurons activated by sustained hypertension: implications for understanding baroreceptor reflex circuitry. J Neurosci 18(1):371-387.

Chastrette N, Pfaff DW, Gibbs RB. 1991. Effects of daytime and nighttime stress on Fos-like immunoreactivity in the paraventricular nucleus of the hypothalamus, the habenula, and the posterior paraventricular nucleus of the thalamus. Brain Res 563(1-2):339-344.

Coleman JE, Huentelman MJ, Kasparov S, Metcalfe BL, Paton JF, Katovich MJ, Semple-Rowland SL, Raizada MK. 2003. Efficient large-scale production and concentration of HIV-1-based lentiviral vectors for use in vivo. Physiol Genomics 12(3):221-228.

Cunningham ET, Jr., Bohn MC, Sawchenko PE. 1990. Organization of adrenergic inputs to the paraventricular and supraoptic nuclei of the hypothalamus in the rat. J Comp Neurol 292(4):651-667.

Dean C. 2005. Sympathoinhibition from ventrolateral periaqueductal gray mediated by the caudal midline medulla. Am J Physiol Regul Integr Comp Physiol 289(5):R1477-1481.

Dun NJ, Dun SL, Chiaia NL. 1993. Hemorrhage induces Fos immunoreactivity in rat medullary catecholaminergic neurons. Brain Res 608(2):223-232.

Enjin A, Rabe N, Nakanishi ST, Vallstedt A, Gezelius H, Memic F, Lind M, Hjalt T, Tourtellotte WG, Bruder C, Eichele G, Whelan PJ, Kullander K. 2010. Identification of novel spinal cholinergic genetic subtypes disclose Chodl and Pitx2 as markers for fast motor neurons and partition cells. J Comp Neurol 518(12):2284-2304.

Erickson JD, Eiden LE, Hoffman BJ. 1992. Expression cloning of a reserpine-sensitive vesicular monoamine transporter. Proc Natl Acad Sci U S A 89(22):10993-10997.

Ericson H, Blomqvist A, Kohler C. 1989. Brainstem afferents to the tuberomammillary nucleus in the rat brain with special reference to monoaminergic innervation. J Comp Neurol 281(2):169-192.

Fekete C, Kelly J, Mihaly E, Sarkar S, Rand WM, Legradi G, Emerson CH, Lechan RM. 2001. Neuropeptide Y has a central inhibitory action on the hypothalamic-pituitary-thyroid axis. Endocrinology 142(6):2606-2613.

Gaillard F, Bonfield S, Gilmour GS, Kuny S, Mema SC, Martin BT, Smale L, Crowder N, Stell WK, Sauve Y. 2008. Retinal anatomy and visual performance in a diurnal cone-rich laboratory rodent, the Nile grass rat (Arvicanthis niloticus). J Comp Neurol 510(5):525-538.

Guyenet PG. 2006. The sympathetic control of blood pressure. Nat Rev Neurosci 7(5):335-346.

Herbert H, Saper CB. 1992. Organization of medullary adrenergic and noradrenergic projections to the periaqueductal gray matter in the rat. J Comp Neurol 315(1):34-52.

Hilton SM, Redfern WS. 1986. A search for brain stem cell groups integrating the defence reaction in the rat. J Physiol 378:213-228.

Hokfelt T, Fuxe K, Goldstein M, Johansson O. 1973. Evidence for adrenaline neurons in the rat brain. Acta Physiol Scand 89(2):286-288.

Hwang, D.Y., Carlezon, W.A., Jr., Isacson, O. & Kim, K.S. 2001. A high-efficiency synthetic promoter that drives transgene expression selectively in noradrenergic neurons. Human gene therapy, 12: 1731-1740.

Imaki T, Shibasaki T, Hotta M, Demura H. 1993. Intracerebroventricular administration of corticotropin-releasing factor induces c-fos mRNA expression in brain regions related to stress responses: comparison with pattern of c-fos mRNA induction after stress. Brain Res 616(1-2):114-125.

James P, Rivier C, Lee S. 2008. Presence of corticotrophin-releasing factor and/or tyrosine hydroxylase in cells of a neural brain-testicular pathway that are labelled by a transganglionic tracer. J Neuroendocrinol 20(2):173-181.

Jansen AS, Wessendorf MW, Loewy AD. 1995. Transneuronal labeling of CNS neuropeptide and monoamine neurons after pseudorabies virus injections into the stellate ganglion. Brain Res 683(1):1-24.

Liu Q, Wong-Riley MT. 2010. Postnatal changes in tryptophan hydroxylase and serotonin transporter immunoreactivity in multiple brainstem nuclei of the rat: implications for a sensitive period. J Comp Neurol 518(7):1082-1097.

Liu Y, Peter D, Roghani A, Schuldiner S, Prive GG, Eisenberg D, Brecha N, Edwards RH. 1992. A cDNA that suppresses MPP+ toxicity encodes a vesicular amine transporter. Cell 70(4):539-551.

Llewellyn-Smith IJ. 2009. Anatomy of synaptic circuits controlling the activity of sympathetic preganglionic neurons. J Chem Neuroanat 38(3):231-239.

Llewellyn-Smith IJ, Martin CL, Marcus JN, Yanagisawa M, Minson JB, Scammell TE. 2003. Orexin-immunoreactive inputs to rat sympathetic preganglionic neurons. Neurosci Lett 351(2):115-119.

Loewy AD, Franklin MF, Haxhiu MA. 1994. CNS monoamine cell groups projecting to pancreatic vagal motor neurons: a transneuronal labeling study using pseudorabies virus. Brain Res 638(1-2):248-260.

Masterson SP, Li J, Bickford ME. 2009. Synaptic organization of the tectorecipient zone of the rat lateral posterior nucleus. J Comp Neurol 515(6):647-663.

Mejias-Aponte CA, Drouin C, Aston-Jones G. 2009. Adrenergic and noradrenergic innervation of the midbrain ventral tegmental area and retrorubral field: prominent inputs from medullary homeostatic centers. J Neurosci 29(11):3613-3626.

Minson J, Llewellyn-Smith I, Neville A, Somogyi P, Chalmers J. 1990. Quantitative analysis of spinally projecting adrenaline-synthesising neurons of C1, C2 and C3 groups in rat medulla oblongata. J Auton Nerv Syst 30(3):209-220.

Montana V, Ni Y, Sunjara V, Hua X, Parpura V. 2004. Vesicular glutamate transporter-dependent glutamate release from astrocytes. J Neurosci 24: 2633–2642.

Murphy AZ, Ennis M, Shipley MT, Behbehani MM. 1994. Directionally specific changes in arterial pressure induce differential patterns of fos expression in discrete areas of the rat brainstem: a double-labeling study for Fos and catecholamines. J Comp Neurol 349(1):36-50.

Nahin RL, Madsen AM, Giesler GJ, Jr. 1983. Anatomical and physiological studies of the gray matter surrounding the spinal cord central canal. J Comp Neurol 220(3):321-335.

Otake K, Ruggiero DA. 1995. Monoamines and nitric oxide are employed by afferents engaged in midline thalamic regulation. J Neurosci 15(3 Pt 1):1891-1911.

Otake K, Ruggiero DA, Nakamura Y. 1995. Adrenergic innervation of forebrain neurons that project to the paraventricular thalamic nucleus in the rat. Brain Res 697(1-2):17-26.

Palazzo E, Rimoli MG, De Chiaro M, Guida F, Melisi D, Curcio A, de Novellis V, Marabese I, Rossi F, Abignente E, Maione S. 2010. Intra-periaqueductal grey microinjections of an imidazo[1,2-b]pyridazine derivative, DM2, affects rostral ventromedial medulla cell activity and shows antinociceptive effect. Neuropharmacology 58(3):660-667.

Pelosi GG, Tavares RF, Antunes-Rodrigues J, Correa FM. 2008. Cardiovascular responses to noradrenaline microinjection in the ventrolateral periaqueductal gray of unanesthetized rats. J Neurosci Res 86(3):712-719.

Peyron C, Luppi PH, Fort P, Rampon C, Jouvet M. 1996. Lower brainstem catecholamine afferents to the rat dorsal raphe nucleus. J Comp Neurol 364(3):402-413.

Phillipson OT, Bohn MC. 1994. C1-3 adrenergic medullary neurones project to the paraventricular thalamic nucleus in the rat. Neurosci Lett 176(1):67-70.

Pickel VM, Chan J, Park DH, Joh TH, Milner TA. 1986. Ultrastructural localization of phenylethanolamine N-methyltransferase in sensory and motor nuclei of the vagus nerve. J Neurosci Res 15(4):439-455.

Pieribone VA, Aston-Jones G, Bohn MC. 1988. Adrenergic and non-adrenergic neurons in the C1 and C3 areas project to locus coeruleus: a fluorescent double labeling study. Neurosci Lett 85(3):297-303.

Pilowsky PM, Morris MJ, Minson JB, West MJ, Chalmers JP, Willoughby JO, Blessing WW. 1987. Inhibition of vasodepressor neurons in the caudal ventrolateral medulla of the rabbit increases both arterial pressure and the release of neuropeptide Y-like immunoreactivity from the spinal cord. Brain Res 420(2):380-384.

Reis DJ, Ruggiero DA, Morrison SF. 1989. The C1 area of the rostral ventrolateral medulla oblongata. A critical brainstem region for control of resting and reflex integration of arterial pressure. Am J Hypertens 2(12 Pt 2):363S-374S.

Sawchenko PE, Bohn MC. 1989. Glucocorticoid receptor-immunoreactivity in C1, C2, and C3 adrenergic neurons that project to the hypothalamus or to the spinal cord in the rat. J Comp Neurol 285(1):107-116.

Schramm LP, Strack AM, Platt KB, Loewy AD. 1993. Peripheral and central pathways regulating the kidney: a study using pseudorabies virus. Brain Res 616(1-2):251-262.

Sevigny CP, Bassi J, Teschemacher AG, Kim KS, Williams DA, Anderson CR, Allen AM. 2008. C1 neurons in the rat rostral ventrolateral medulla differentially express vesicular monoamine transporter 2 in soma and axonal compartments. Eur J Neurosci 28(8):1536-1544.

Sharp FR, Sagar SM, Hicks K, Lowenstein D, Hisanaga K. 1991. c-fos mRNA, Fos, and Fos-related antigen induction by hypertonic saline and stress. J Neurosci 11(8):2321-2331.

Stornetta RL. 2009. Neurochemistry of bulbospinal presympathetic neurons of the medulla oblongata. J Chem Neuroanat 38(3):222-230.

Stornetta RL, Akey PJ, Guyenet PG. 1999. Location and electrophysiological characterization of rostral medullary adrenergic neurons that contain neuropeptide Y mRNA in rat medulla. J Comp Neurol 415(4):482-500.

Stornetta RL, Sevigny CP, Guyenet PG. 2002. Vesicular glutamate transporter DNPI/VGLUT2 mRNA is present in C1 and several other groups of brainstem catecholaminergic neurons. J Comp Neurol 444(3):191-206.

Teschemacher AG, Wang S, Lonergan T, Duale H, Waki H, Paton JF, Kasparov S. 2005. Targeting specific neuronal populations using adeno- and lentiviral vectors: applications for imaging and studies of cell function. Exp Physiol 90(1):61-69.

Tjen ALSC, Li P, Longhurst JC. 2006. Midbrain vlPAG inhibits rVLM cardiovascular sympathoexcitatory responses during electroacupuncture. Am J Physiol Heart Circ Physiol 290(6):H2543-2553.

Weihe E, Schäfer MKH, Erickson JD, Eiden LE. 1994. Localization of vesicular monoamine transporter isoforms (VMAT1 and VMAT2) to endocrine cells and neurons in rat. J Mol Neurosci 5: 149–164.

Weihe E, Schutz B, Hartschuh W, Anlauf M, Schafer MK, Eiden LE. 2005. Coexpression of cholinergic and noradrenergic phenotypes in human and nonhuman autonomic nervous system. J Comp Neurol 492(3):370-379.

Wittmann G, Liposits Z, Lechan RM, Fekete C. 2002. Medullary adrenergic neurons contribute to the neuropeptide Y-ergic innervation of hypophysiotropic thyrotropin-releasing hormone-synthesizing neurons in the rat. Neurosci Lett 324(1):69-73.

Wittmann G, Liposits Z, Lechan RM, Fekete C. 2004. Medullary adrenergic neurons contribute to the cocaine- and amphetamine-regulated transcript-immunoreactive innervation of thyrotropin-releasing hormone synthesizing neurons in the hypothalamic paraventricular nucleus. Brain Res 1006(1):1-7.

Figure Legends

Table 1: Description of antibodies used for immunohistochemistry

Table 2: Comparative contributions of C1 and C3 neuronal processes within the framework of overall CNS PNMT distribution. Semi-quantitation ranges from sparse or single varicose axons (+) to the highest density of varicose processes observed (++++). Please note that the scale of semi-quantitation is relative to either overall PNMT density as detailed by Björklund and Hökfelt (1984; in the overall density column) or density of C3 processes (C3 column). C1 contributions, as detailed by Card et al. (2006) are qualitative only, where * indicates a region reported to contain C1 processes, and blank fields represent regions which weren't reported. "x" represents regions which were investigated in the current study, but did not contain C3 processes.

Figure 1: Representative fluorescent micrograph illustrating the caudal (row A) and rostral (row B) extent of the lentiviral injection site, just ventral to the fourth ventricle (4V). A majority of tyrosine hydroxylase (TH)-ir (magenta) C3 neurons are expressing green fluorescent protein (GFP; green) subsequent to lentiviral infection. Scale bar represents 200µm.

Figure 2: A) Confocal micrograph depicting GFP-ir C3 processes in an oblique horizontal section through the mid-thoracic spinal cord at the level of Lamina X and the central canal (cc). Panels B-D also feature transverse sections of lamina X showing GFP-ir processes (green) and choline acetyltransferase (ChAT)-ir neurons (magenta) at the levels of B) mid-cervical, C) lumbar, and D) sacral spinal cord. Panel E depicts GFP-ir processes in a transverse section through the intermediolateral cell column (IML) of the mid-thoracic spinal cord. Panel F depicts GFP-ir processes in the IML of the mid-thoracic spinal cord overlapping with ChAT-ir sympathetic preganglionic neurons. A 100x magnification enlargement of the dotted box region imaged at a low depth of field shows colocalization of G) GFP-ir, H) vesicular glutamate transporter 2 (VGluT2)-ir, and J) vesicular monoamine transporter 2 (VMAT2)-ir in C3 axon varicosities. Panels I and K are merged images with GFP and VGluT2 (I) or VMAT2 (K). Arrowheads indicate varicosities co-expressing GFP, VGlut2 and VMAT2.

Scale bars represent 100µm (panels A-E) or 20µm where indicated.

Figure 3: Top Row: Nissl stained coronal sections sampled at various levels throughout the brainstem. Lettered boxes correspond to representative confocal micrographs illustrating GFP-ir C3 processes (green) A) in the nucleus of the solitary tract (medial part; TH-ir C2 neurons visible in magenta), B) interacting with the surface of the fourth ventricle, C) in the rostral ventrolateral medulla (TH-ir C1 neurons visible in magenta), D) travelling along the ventral surface, E) in raphe obscurus (tryptophan hydroxylase [TrOH]-ir B2 neurons in magenta), F) raphe pallidus (TrOH-ir B1 neurons in magenta), G) area postrema, H) dorsal motor nucleus of the vagus (ChAT-ir motor neurons in magenta), and I) caudal ventrolateral medulla (TH-ir A1 neurons in magenta). Scale bar represents 100µm for confocal images. 4V: fourth ventricle; 12N: hypoglossal nucleus; Rob: raphe obscurus; Amb: nucleus ambiguus; mNTS: nucleus of the solitary tract (medial); DMX: dorsal motor nucleus of the vagus; RVLM: rostral ventromedial medulla; Rpa: raphe pallidus; CVLM: caudal ventrolateral medulla.

Figure 4: Top row: Nissl stained coronal sections sampled at various levels throughout the pons/midbrain. Lettered boxes correspond with confocal micrographs illustrating GFP-ir C3 processes (green) in A) ventrolateral periaqueductal gray, B) dorsal raphe nucleus (TrOH-ir B6/B7 neurons visible in magenta), C) supraoculomotor periaqueductal gray, D) ventral tegmental area (A10 neurons visible in magenta), E) Kölliker-Fuse nucleus (TH-ir A7 neurons visible in magenta), F) lateral parabrachial nucleus, G) medial parabrachial nucleus (contributing to dense TH-ir processes visible in magenta), H) locus coeruleus (TH-ir A6 neurons visible in magenta), and I) raphe magnus (TrOH-ir B3 neurons visible in magenta). Scale bar represents 100µm for confocal images. Aq: aqueduct; RtTg: reticulotegmental nucleus of the pons; 5: trigeminal nucleus; 4V: fourth ventricle; vlPAG: ventrolateral periaqueductal gray; Su3PAG: supraoculomotor periaqueductal gray; VTA: ventral tegmental area, LPB: lateral parabrachial nucleus; MPB: medial parabrachial nucleus; LC: locus coeruleus.

Figure 5: Nissl stained coronal section sampled from caudal forebrain (top left panel). Lettered boxes correspond to representative confocal micrographs illustrating GFP-ir C3 processes in A) paraventricular nucleus of the thalamus, B) mediodorsal thalamic nucleus, C) posterior hypothalamic nucleus, D) dorsomedial hypothalamic nucleus, E) arcuate hypothalamic nucleus (medial posterior part), F) medial tuberal nucleus, G) terete hypothalamic nucleus, and H) medial amygdaloid nucleus. Scale bar represents 100µm for confocal images. D3V: dorsal third

ventricle; VM: ventromedial thalamic nucleus; 3V: third ventricle; PVT: paraventricular nucleus of the thalamus; MDT: mediodorsal thalamic nucleus; PH: posterior hypothalamic nucleus; DMH: dorsomedial hypothalamic nucleus; Arc: arcuate hypothalamic nucleus.

Figure 6: Top row: Nissl stained coronal sections sampled at various levels of the diencephalon, with the third ventricle visible at center. Lettered boxes correspond with representative confocal micrographs illustrating GFP-ir C3 processes in A) periventricular nucleus of the hypothalamus, B) retrochiasmatic nucleus, C) paraventricular nucleus of the thalamus, D) lateral hypothalamus, E) supraoptic nucleus, F) paraventricular nucleus of the hypothalamus (medial parvicellular part), G) median eminence H) paraventricular nucleus of the hypothalamus (posterior part), and I) arcuate hypothalamic nucleus. Scale bar represents 100µm for confocal images. och: optic chiasm; sod: supraoptic decussation; 3V: third ventricle; VMH: ventromedial hypothalamic nucleus; PeH: periventricular nucleus of the hypothalamus; RCh: retrochiasmatic nucleus; PVT: paraventricular nucleus of the thalamus; LH: lateral hypothalamus; SO: supraoptic nucleus; PVN: paraventricular nucleus of the hypothalamus; ME: median eminence; Arc: arcuate hypothalamic nucleus.

Figure 7: Nissl stained coronal section of rostral forebrain taken at the level anterior and ventral to the third ventricle (top left panel). Lettered boxes correspond with representative confocal micrographs illustrating GFP-ir C3 processes in A) bed nucleus of the stria terminalis, B) median preoptic nucleus, C) medial preoptic nucleus, and D) organum vasculosum of lamina terminalis. Scale bar represents 100µm for confocal images. LV: lateral ventricle; aca: anterior commisure (anterior part); och: optic chiasm; BST: bed nucleus of the stria terminalis; OVLT: organum vasculosum of lamina terminalis.

Figure 8: High magnification confocal micrographs of GFP-ir (green) and VGlut2-ir (majenta) axon varicosities in the dorsal motor nucleus of the vagus (DMX; panels A-C), paraventricular nucleus of the thalamus (PVT; panels D-F), paraventricular nucleus of the hypothalamus (PVN; panels G-I), and area postrema (AP; panels J-L). Panel A illustrates a GFP-ir (green) axon in close proximity to a ChAT-ir (blue) neuron in DMX. Panels C, F, I, and L show merged GFP-ir (green) and VGluT-ir (majenta) images. Arrowheads indicate axon varicosities double-labeled for GFP-ir and VGluT2-ir (overlapping channels appear white). Scale bars represent 20µm.

Primary Antibodies			
Antigen	*Immunogen*	*Manufacturer; Species Antibody Was Raised In; Mono- vs. Polyclonal; Catalog Number*	*Dilution Used*
Green Fluorescent Protein	recombinant full length protein	Abcam (Redfern, Australia); chicken polyclonal; #AB13970	1:5,000
Tyrosine Hydroxylase	denatured enzyme from rat pheochromocytoma	Chemicon International (Temecula, CA); rabbit polyclonal; #AB152	1:2,500
Tryptophan Hydroxylase	recombinant rabbit enzyme	Sigma-Aldrich (St. Louis, MO); mouse monoclonal #T0678	1:5,000
Choline Acetyltransferase	human placental enzyme	Chemicon International (Temecula, CA); goat polyclonal; #AB144P	1:1,000
Vesicular Monoamine Transporter 2	synthetic peptide (C-terminus) from rat protein (CTQNNVQSYPIGDDEESESD)	Phoenix Laboratories (Belmont, CA); rabbit polyclonal; #H-V004	1:5,000
Vesicular Glutamate Transporter 2	synthetic peptide from rat protein (VQESAQDAYSYKDRDDYS)	Chemicon International (Temecula, CA); guinea pig polyclonal; #AB5907	1:2,500

Secondary Antibodies		
Antibody	*Manufacturer; Catalog Number*	*Dilution Used*
Alexa Fluor® 488 conjugated goat anti-chicken IgG	Invitrogen Australia (Mulgrave, Australia) #A-11039	1:500
Cy™3 conjugated AffiniPure donkey anti-rabbit IgG	Jackson Immunoresearch (West Grove, PA) #711-165-152	1:500
Cy™3 conjugated AffiniPure donkey anti-mouse IgG	Jackson Immunoresearch (West Grove, PA) #715-165-151	1:500
Cy™5 conjugated AffiniPure donkey anti-goat IgG	Jackson Immunoresearch (West Grove, PA) #705-175-003	1:500
Biotin-SP conjugated AffiniPure donkey anti-guinea pig IgG	Jackson Immunoresearch (West Grove, PA) #706-065-148	1:500
Cy™5 conjugated streptavidin	Jackson Immunoresearch (West Grove, PA) #016-170-084	1:2000

Regions Expressing PNMT (CNS)			Overall Density	C1	C3
Telencephalon		Anterior Olfactory Nucleus	+		+
		Septal Nucleus	+		+
		Nucleus Tractus Diagonalis	+		+
		Bed Nucleus of Stria Terminalis	+++		+
		Central Amygdaloid Nucleus	+		x
		Medial Amygdaloid Nucleus	++		++
Diencephalon	Hypothalamus	Organum Vasculosum of Lamina Terminalis	+++		++
		Suprachiasmatic Nucleus	+++		++
		Arcuate Nucleus	++	*	++
		Lateral Hypothalamus	++	*	+
		Perifornical Area	++	*	+
		Medial Tuberal Nucleus and Terete Nucleus	++++	*	+
		Paraventricular Nucleus	++++	*	+++
		Periventricular Nucleus	+++		+++
		Dorsomedial Nucleus	++	*	++
		Medial Preoptic Nucleus	++	*	++
		Anterior Hypothal. Nucleus	+		x
		Ventromedial Nucleus	+		x
		Retrochiasmatic Nucleus	++		++
		Median Eminence	++	*	+
		Supraoptic Nucleus	+	*	++
	Thalamus	Periventricular Nucleus	++++	*	++++
		Rhomboid Nucleus	+++		+++
	Other	Supramamillary Region	++		x
Mesencephalon and Pons		Lateral Periaqueductal Gray	+++	*	++
		Ventrolateral Periaqueductal Gray	+++	*	++++
		Substantia Nigra (Zona Compacta)	+		x
		Ventral Tegmental Area	++		++
		Dorsal Raphé	++		++
		Central Superior Nucleus	++		x
		Pontine Reticular Formation	+		x
		Locus Coeruleus	+++	*	++
		A7 / Kölliker Fuse Nucleus	+++		++
		Parabrachial Nucleus (Dorsal)	+++		+++
		Superior Olive	++		x
		Corpus Trapezoideum	++		x
		A5 Nucleus	+++		x
Cerebellum		Purkinje Layer	++		x
Medulla Oblongata		Reticular Gigantocellular Nucleus	+		x
		Raphé Pallidus	+++	*	+
		Raphé Magnus	+++		+
		Pyramidal Tract	++		x
		Raphé Obscurus	++	*	+
		Dorsal Motor Nucleus of the Vagus	++++	*	+++
		Nucleus of the Solitary Tract (Commissural)	++++	*	+++
		Area Postrema	++++	*	++++
		Nucleus of the Solitary Tract (Medial)	+++	*	++++

		Nucleus Intercalatus	++		x
		Caudal Ventrolateral Medulla (A1)	+++	*	++
		Rostral Ventrolateral Medulla	++	*	++
		Reticular Nucleus	+	*	x
		Lateral Reticular Nucleus	+	*	x
		Decussation of the Pyramids	+		x
		Nucleus Ambiguus		*	x
Spinal Cord	Cervical	Lamina X	++		++
	Thoracic	Lamina X	++++	*	++++
		Intermediolateral Cell Column (Lamina IX)	++++	*	++++
	Lumbar	Lamina X	++		++
	Sacral	Lamina X	++		+

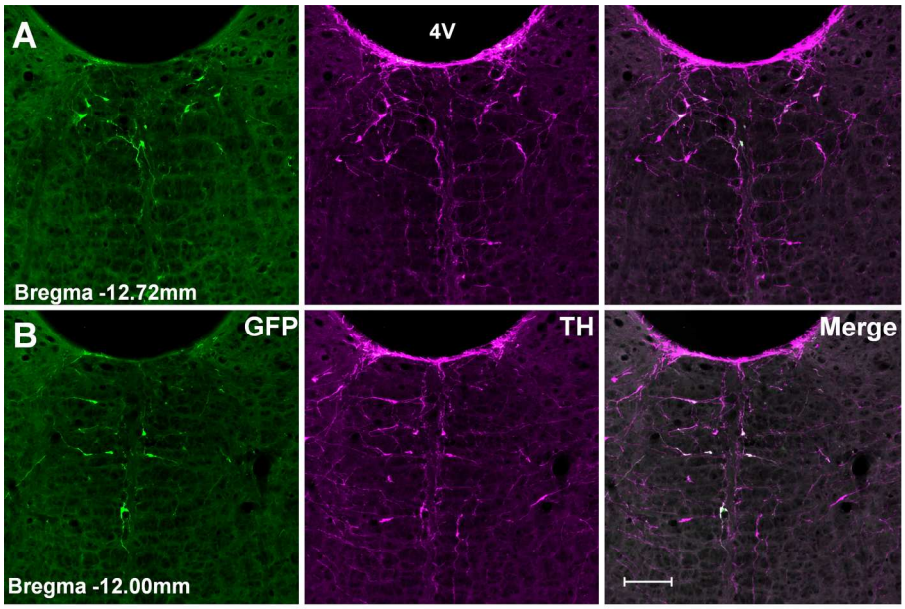

Figure 1: Representative fluorescent micrograph illustrating the caudal (row A) and rostral (row B) extent of the lentiviral injection site, just ventral to the fourth ventricle (4V). A majority of tyrosine hydroxylase (TH)-ir (magenta) C3 neurons are expressing green fluorescent protein (GFP; green) subsequent to lentiviral infection. Scale bar represents 200μm.
171x230mm (300 x 300 DPI)

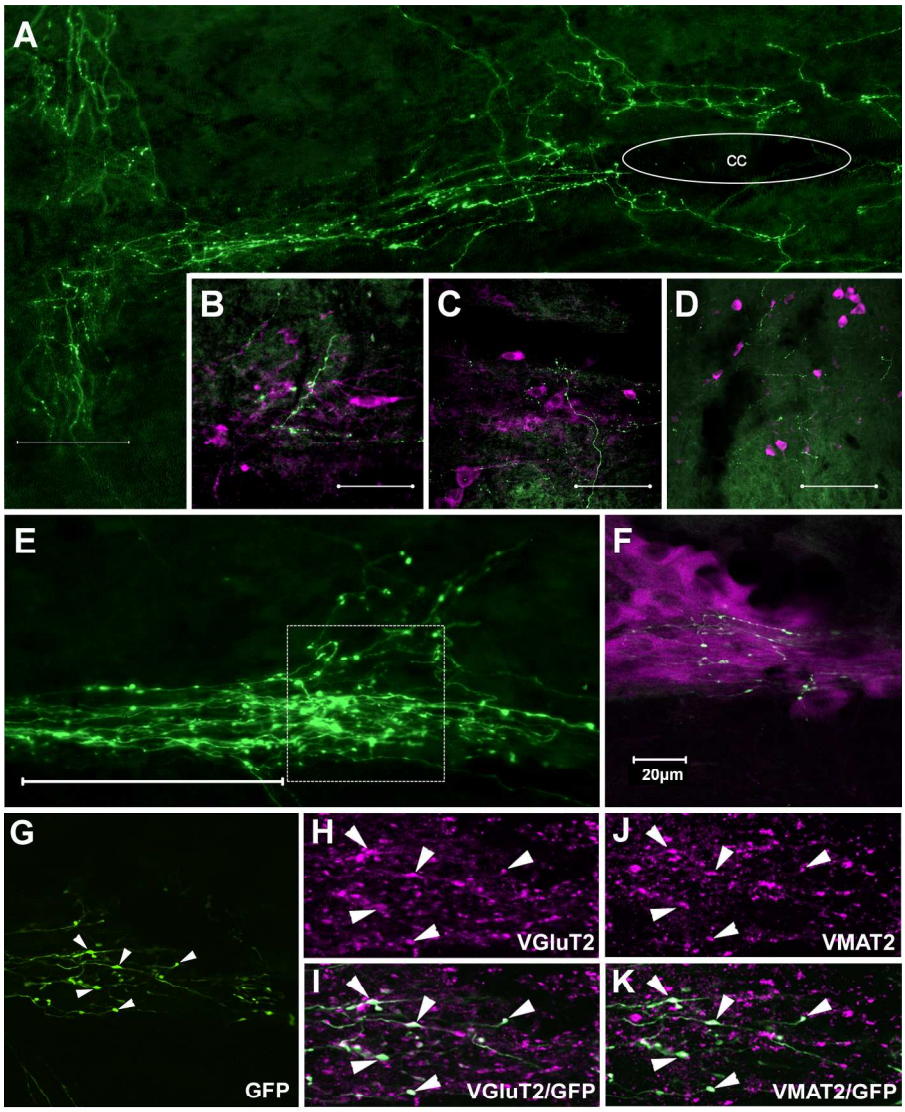

Figure 2: A) Confocal micrograph depicting GFP-ir C3 processes in an oblique horizontal section through the mid-thoracic spinal cord at the level of Lamina X and the central canal (cc). Panels B-D also feature transverse sections of lamina X showing GFP-ir processes (green) and choline acetyltransferase (ChAT)-ir neurons (magenta) at the levels of B) mid-cervical, C) lumbar, and D) sacral spinal cord. Panel E depicts GFP-ir processes in a transverse section through the intermediolateral cell column (IML) of the mid-thoracic spinal cord. Panel F depicts GFP-ir processes in the IML of the mid-thoracic spinal cord overlapping with ChAT-ir sympathetic preganglionic neurons. A 100x magnification enlargement of the dotted box region imaged at a low depth of field shows colocalization of G) GFP-ir, H) vesicular glutamate transporter 2 (VGluT2)-ir, and J) vesicular monoamine transporter 2 (VMAT2)-ir in C3 axon varicosities. Panels I and K are merged images with GFP and VGluT2 (I) or VMAT2 (K). Arrowheads indicate varicosities co-expressing GFP, VGlut2 and VMAT2.
Scale bars represent 100µm (panels A-E) or 20µm where indicated.

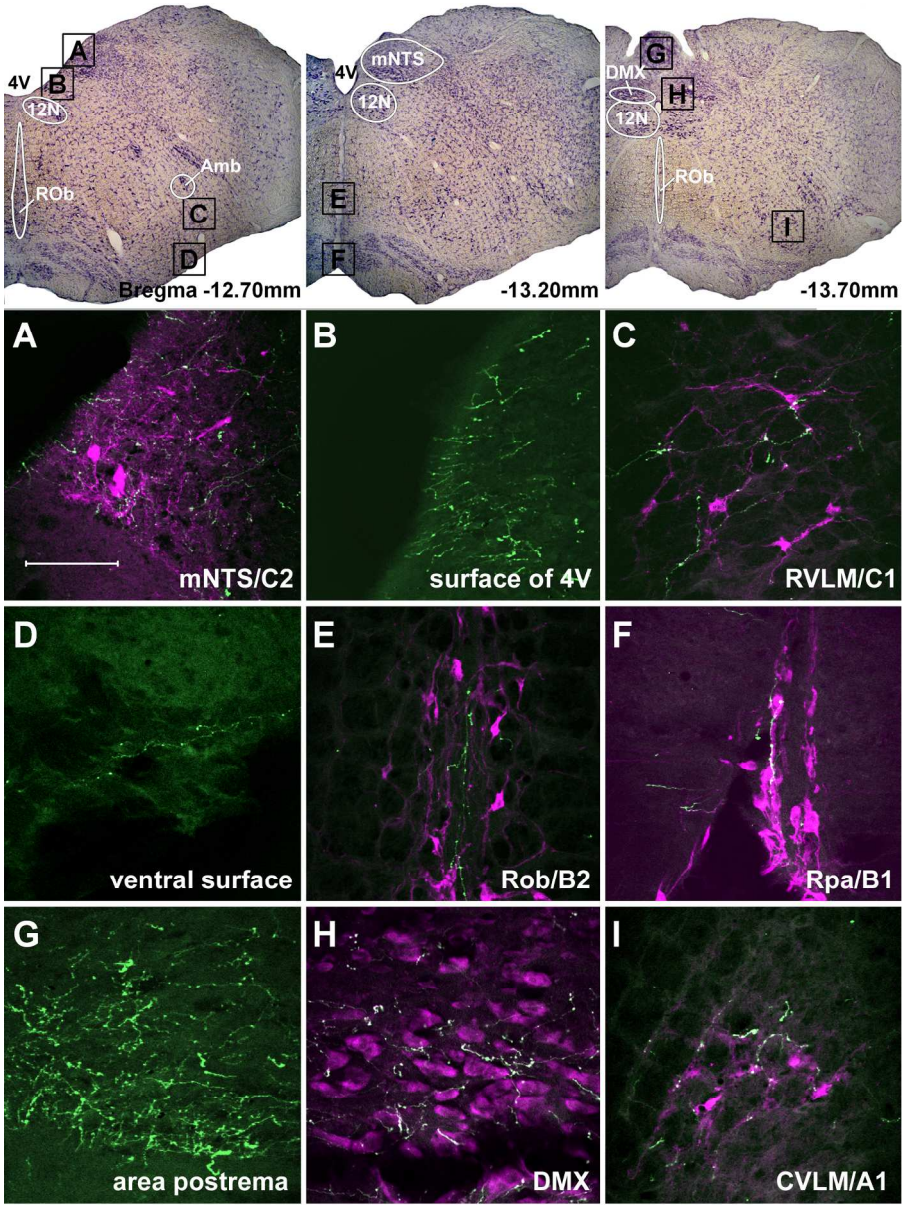

Figure 3: Top Row: Nissl stained coronal sections sampled at various levels throughout the brainstem. Lettered boxes correspond to representative confocal micrographs illustrating GFP-ir C3 processes (green) A) in the nucleus of the solitary tract (medial part; TH-ir C2 neurons visible in magenta), B) interacting with the surface of the fourth ventricle, C) in the rostral ventrolateral medulla (TH-ir C1 neurons visible in magenta), D) travelling along the ventral surface, E) in raphe obscurus (tryptophan hydroxylase [TrOH]-ir B2 neurons in magenta), F) raphe pallidus (TrOH-ir B1 neurons in magenta), G) area postrema, H) dorsal motor nucleus of the vagus (ChAT-ir motor neurons in magenta), and I) caudal ventrolateral medulla (TH-ir A1 neurons in magenta). Scale bar represents 100μm for confocal images. 4V: fourth ventricle; 12N: hypoglossal nucleus; Rob: raphe obscurus; Amb: nucleus ambiguus; mNTS: nucleus of the solitary tract (medial); DMX: dorsal motor nucleus of the vagus; RVLM: rostral ventromedial medulla; Rpa: raphe pallidus; CVLM: caudal ventrolateral medulla.
171x230mm (300 x 300 DPI)

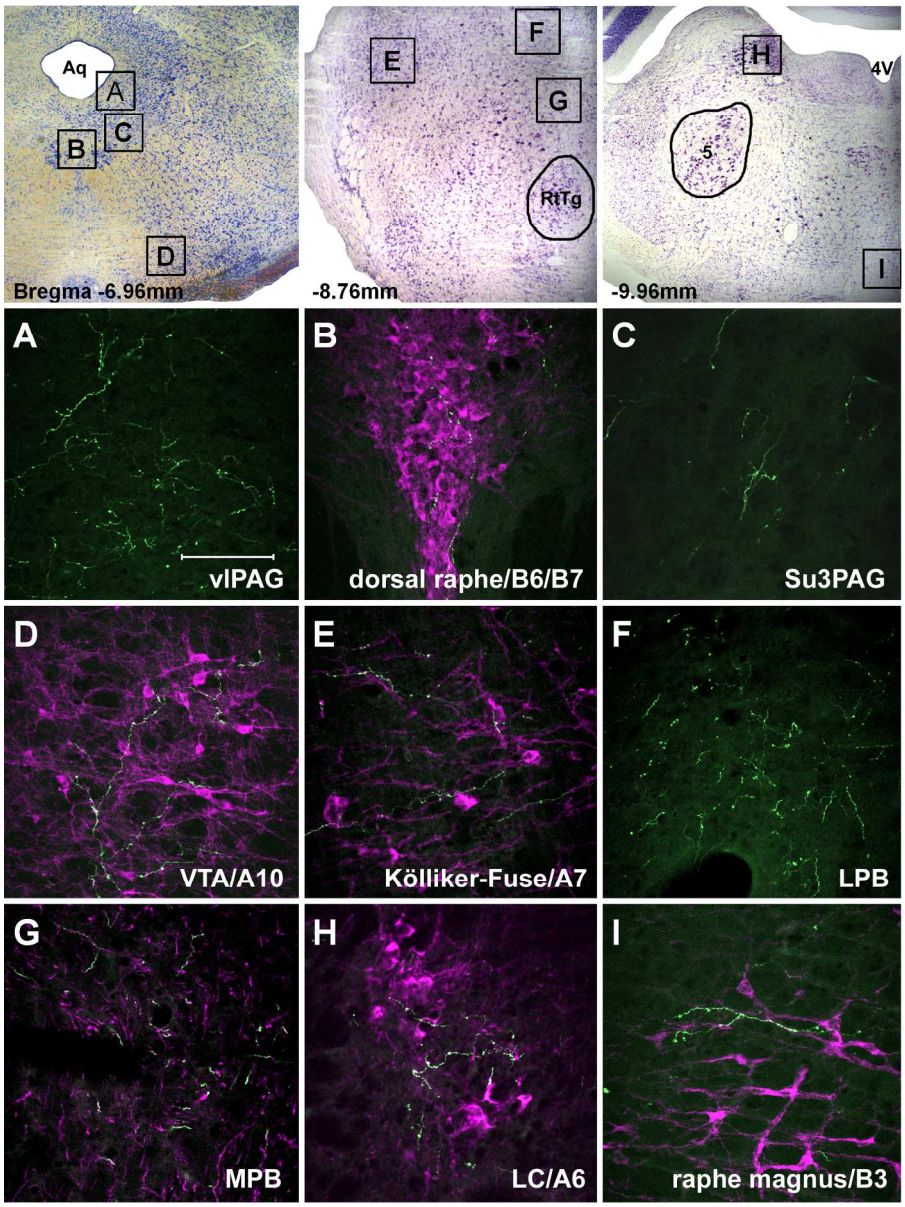

Figure 4: Top row: Nissl stained coronal sections sampled at various levels throughout the pons/midbrain. Lettered boxes correspond with confocal micrographs illustrating GFP-ir C3 processes (green) in A) ventrolateral periaqueductal gray, B) dorsal raphe nucleus (TrOH-ir B6/B7 neurons visible in magenta), C) supraoculomotor periaqueductal gray, D) ventral tegmental area (A10 neurons visible in magenta), E) Kölliker-Fuse nucleus (TH-ir A7 neurons visible in magenta), F) lateral parabrachial nucleus, G) medial parabrachial nucleus (contributing to dense TH-ir processes visible in magenta), H) locus coeruleus (TH-ir A6 neurons visible in magenta), and I) raphe magnus (TrOH-ir B3 neurons visible in magenta). Scale bar represents 100μm for confocal images. Aq: aqueduct; RtTg: reticulotegmental nucleus of the pons; 5: trigeminal nucleus; 4V: fourth ventricle; vlPAG: ventrolateral periaqueductal gray; Su3PAG: supraoculomotor periaqueductal gray; VTA: ventral tegmental area, LPB: lateral parabrachial nucleus; MPB: medial parabrachial nucleus; LC: locus coeruleus.
171x230mm (300 x 300 DPI)

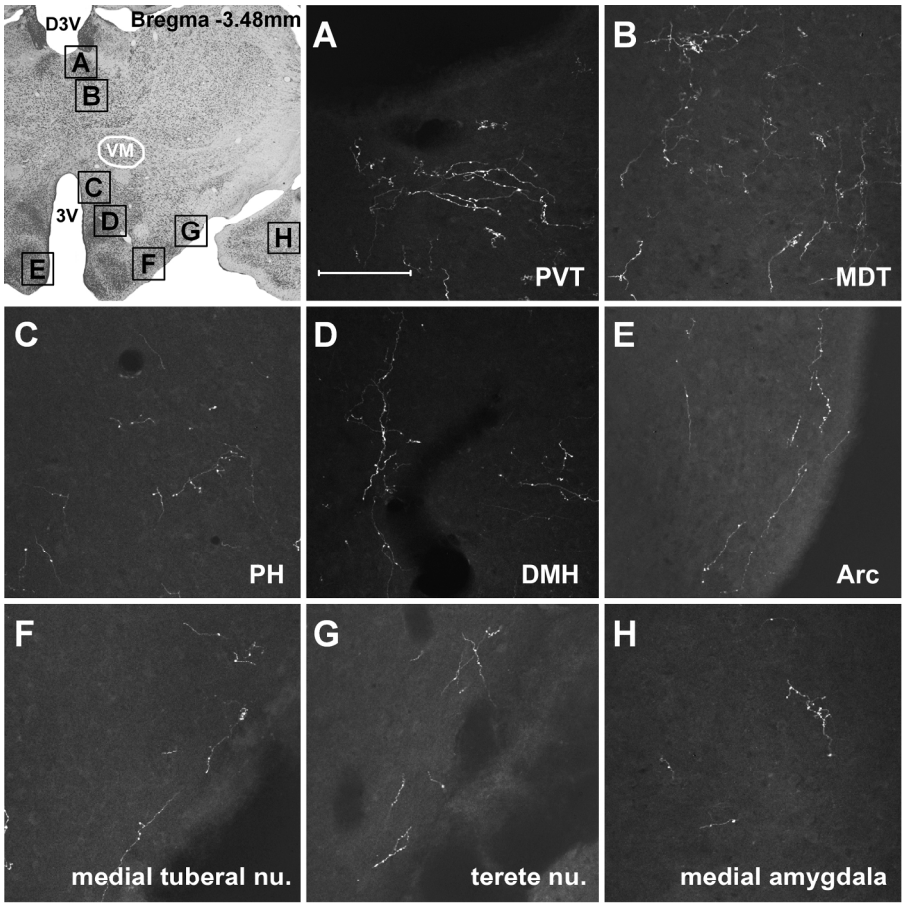

Figure 5: Nissl stained coronal section sampled from caudal forebrain (top left panel). Lettered boxes correspond to representative confocal micrographs illustrating GFP-ir C3 processes in A) paraventricular nucleus of the thalamus, B) mediodorsal thalamic nucleus, C) posterior hypothalamic nucleus, D) dorsomedial hypothalamic nucleus, E) arcuate hypothalamic nucleus (medial posterior part), F) medial tuberal nucleus, G) terete hypothalamic nucleus, and H) medial amygdaloid nucleus. Scale bar represents 100μm for confocal images. D3V: dorsal third ventricle; VM: ventromedial thalamic nucleus; 3V: third ventricle; PVT: paraventricular nucleus of the thalamus; MDT: mediodorsal thalamic nucleus; PH: posterior hypothalamic nucleus; DMH: dorsomedial hypothalamic nucleus; Arc: arcuate hypothalamic nucleus.
171x230mm (300 x 300 DPI)

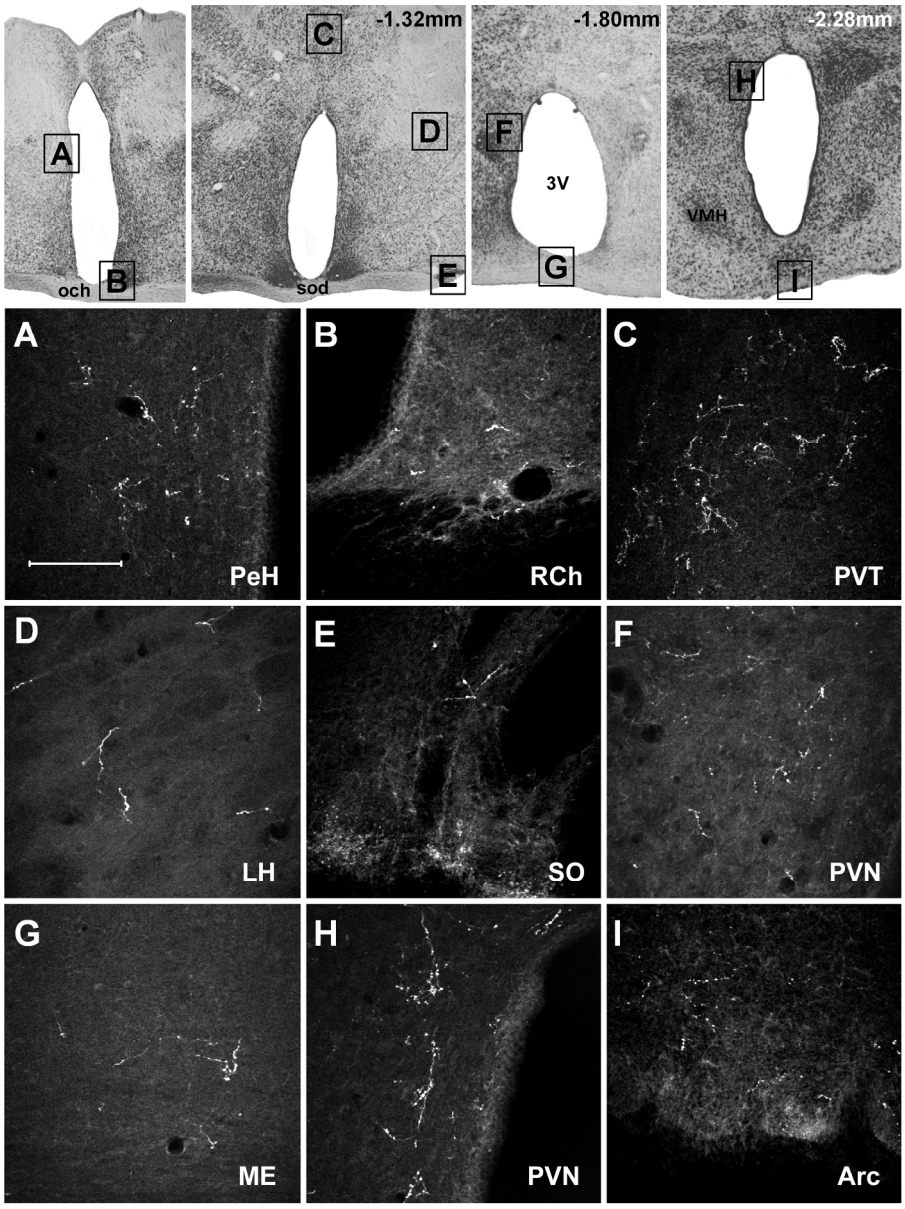

Figure 6: Top row: Nissl stained coronal sections sampled at various levels of the diencephalon, with the third ventricle visible at center. Lettered boxes correspond with representative confocal micrographs illustrating GFP-ir C3 processes in A) periventricular nucleus of the hypothalamus, B) retrochiasmatic nucleus, C) paraventricular nucleus of the thalamus, D) lateral hypothalamus, E) supraoptic nucleus, F) paraventricular nucleus of the hypothalamus (medial parvicellular part), G) median eminence H) paraventricular nucleus of the hypothalamus (posterior part), and I) arcuate hypothalamic nucleus. Scale bar represents 100μm for confocal images. och: optic chiasm; sod: supraoptic decussation; 3V: third ventricle; VMH: ventromedial hypothalamic nucleus; PeH: periventricular nucleus of the hypothalamus; RCh: retrochiasmatic nucleus; PVT: paraventricular nucleus of the thalamus; LH: lateral hypothalamus; SO: supraoptic nucleus; PVN: paraventricular nucleus of the hypothalamus; ME: median eminence; Arc: arcuate hypothalamic nucleus.
171x230mm (300 x 300 DPI)

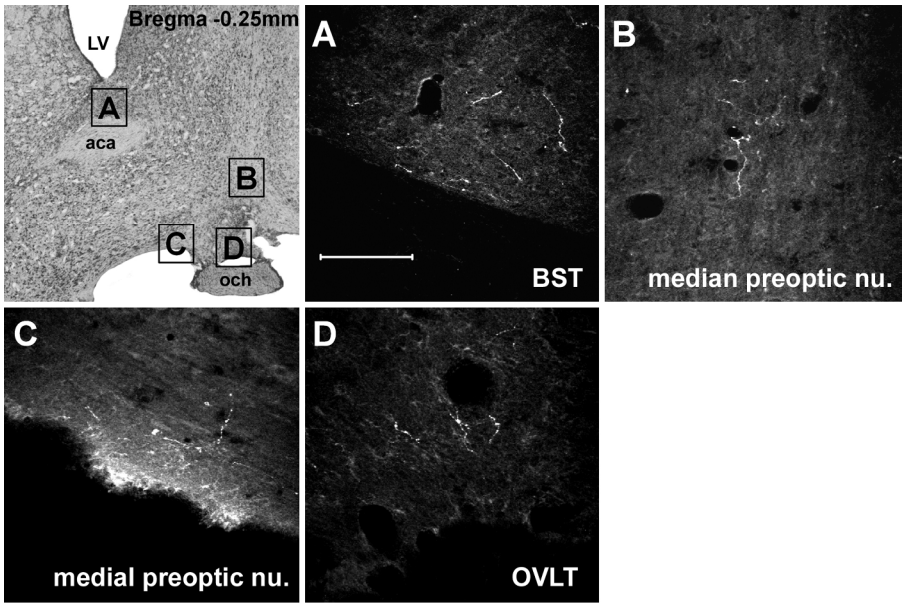

Figure 7: Nissl stained coronal section of rostral forebrain taken at the level anterior and ventral to the third ventricle (top left panel). Lettered boxes correspond with representative confocal micrographs illustrating GFP-ir C3 processes in A) bed nucleus of the stria terminalis, B) median preoptic nucleus, C) medial preoptic nucleus, and D) organum vasculosum of lamina terminalis. Scale bar represents 100μm for confocal images. LV: lateral ventricle; aca: anterior commisure (anterior part); och: optic chiasm; BST: bed nucleus of the stria terminalis; OVLT: organum vasculosum of lamina terminalis.
171x230mm (300 x 300 DPI)

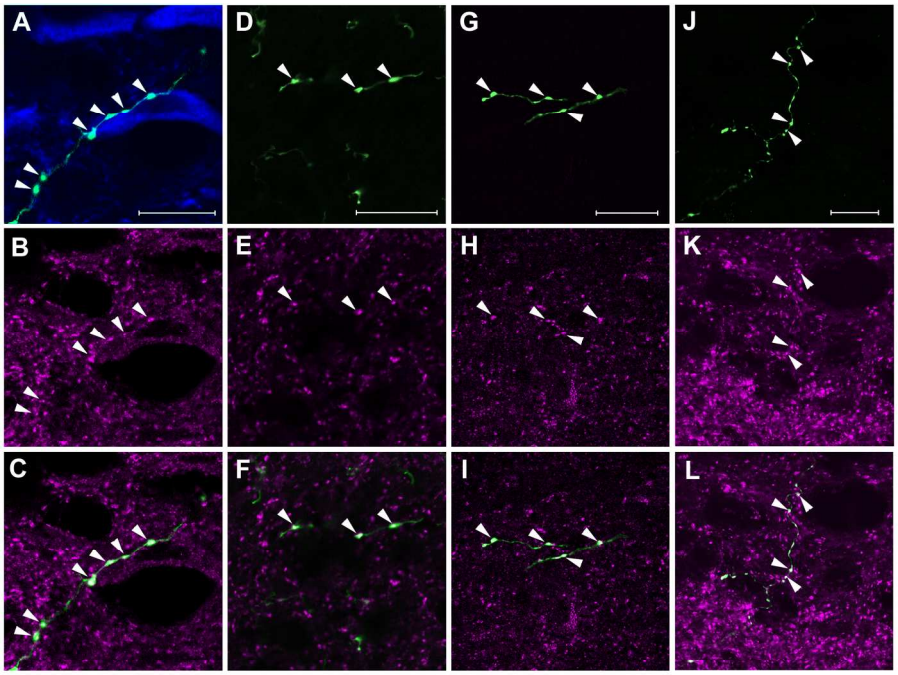

Figure 8: High magnification confocal micrographs of GFP-ir (green) and VGlut2-ir (majenta) axon varicosities in the dorsal motor nucleus of the vagus (DMX; panels A-C), paraventricular nucleus of the thalamus (PVT; panels D-F), paraventricular nucleus of the hypothalamus (PVN; panels G-I), and area postrema (AP; panels J-L). Panel A illustrates a GFP-ir (green) axon in close proximity to a ChAT-ir (blue) neuron in DMX. Panels C, F, I, and L show merged GFP-ir (green) and VGluT-ir (majenta) images. Arrowheads indicate axon varicosities double-labeled for GFP-ir and VGluT2-ir (overlapping channels appear white). Scale bars represent 20µm.
171x230mm (300 x 300 DPI)